Computational Mechanics 32 (2003) 392–400 © Springer-Verlag 2003
DOI 10.1007/s00466-003-0505-5

Stress intensity factor analysis of friction sliding at discontinuity interfaces and junctions

A.-V. Phan, J. A. L. Napier, L. J. Gray, T. Kaplan

Abstract A stress intensity factor (SIF) analysis for two-dimensional fractures with frictional contact (crack friction) is presented. This analysis is carried out using the symmetric-Galerkin boundary element method, and a modified quarter-point crack tip element. As in case of non-contact fracture, it is shown that highly accurate SIFs can be obtained, even with the simple Displacement Correlation SIF technique. Moreover, with the modified crack tip element, the mesh on the crack does not need to be excessively refined in order to achieve high accuracy. This meshing advantage is especially important in the context of the nonlinear frictional contact problem, as the computing time for the iterative process strongly depends on the number of elements used. Several numerical examples are presented and the SIF results are compared with available analytical or reference solutions.

Keywords Stress intensity factor, Crack friction, Modified quarter-point element, Boundary element method, Symmetric-Galerkin approximation

1 Introduction

The two principal approaches for computational fracture analysis are the finite element method (FEM) (e.g., [1]) and boundary element method (BEM) [2–5]. The key feature of the integral equation approach is that only the boundary of the domain is discretized and only boundary quantities are determined. As a result, for fracture analysis, the singular stress field ahead of the crack is not approximated, and moreover, remeshing a propagating crack is easier.

In both finite and boundary element modeling of discrete cracks, the standard approach consists of incorporating the critical stress singularity and $\sqrt{r}$ displacement behavior at the crack tip by means of the 'quarter-point' (QP) element [6, 7]. Use of this QP element at the crack tip has significantly improved the accuracy of SIF calculations (e.g., [8, 9]). Nevertheless, in either finite or boundary element analyses, the prediction of K_{II} and K_{III} has not been nearly as accurate as for K_I. Recently, Gray and Paulino [10] have proved that, for an arbitrary crack geometry, a constraint exists in the series expansion of the crack opening displacement at the tip. As discussed in [10], the QP element in general fails to satisfy this constraint, and this has led to the development of an improved QP element [11]. It was demonstrated in [11] that the accuracy of the computed crack tip SIFs can be significantly improved by using the modified quarter-point (MQP) element.

Contact friction boundary conditions arise in problems relating to rolling and sliding between machine components or other bodies [12–14] and are ubiquitous in the fields of earthquake science, rock mechanics and geotechnical engineering, where multiple interacting faults and discontinuities are present. The numerical treatment of these problems often presents a number of difficulties in that boundary conditions are specified in the form of inequality constraints rather than in terms of fixed tractions or displacements. Further difficulties arise when either kinked cracks or multiple intersecting junctions are considered. For two-dimensional (2-D) problems, a rosette of interacting wedge structures have to be analyzed with, in general, power law displacement functions on each wedge face. Three-dimensional (3-D) junctions can obviously be considerably more complicated and demanding. Numerical methods that have been employed for crack friction problems include FEM [15], BEM using an integral equation for the resultant forces along a crack [16–18], muti-domain BEM [19], dual BEM [20], displacement discontinuity method (DDM) [21–24], and Symmetric-Galerkin BEM (SGBEM) [25].

Note that all the BEM and the DMM are collocation methods as they employ collocation at either boundary nodes or internal nodes (internal collocation), while the SGBEM employs a Galerkin approximation. The major disadvantage associated with a collocation scheme is that the relaxation of continuity requirements at element boundaries and junctions will lead to singularities in the

A.-V. Phan (✉)
Department of Mechanical Engineering,
University of South Alabama, Mobile, AL 36688-0002, USA
e-mail: vphan@jaguar1.usouthal.edu

J. A. L. Napier
CSIR, Division of Mining Technology,
Auckland Park 2006, Johannesburg, South Africa

L. J. Gray, T. Kaplan
Computer Science and Mathematics Division,
Oak Ridge National Laboratory, Oak Ridge, TN 37831-6367, USA

This research was supported in part by the University of South Alabama Research Council, and by the Applied Mathematical Sciences Research Program of the Office of Mathematical, Information, and Computational Sciences, U.S. Department of Energy under contract DE-AC05-00OR22725 with UT-Battelle, LLC.

stress field in the vicinity of these points. If multiple, closely spaced crack assemblies are to be analyzed, this can, in certain cases, lead to numerical difficulties. The SGBEM offers two key advantages following from the Galerkin procedure. First, unlike collocation, there is no smoothness requirement on the displacement [26, 27] in order to evaluate the hypersingular integral; thus, standard *continuous* elements can be employed. The Galerkin approach can therefore easily exploit the highly effective quarter-point quadratic element to accurately capture the crack tip behavior. Second, the weighted averaging formulation of Galerkin, by avoiding direct collocation at corners and junction points, provides a smoother solution in the neighborhood of geometric discontinuities. This may explain why a simple frictional contact algorithm such as the one proposed in Reference [25] can be employed with the SGEBM to successfully treat crack friction problems.

The focus of this paper is on SIF evaluation for 2-D crack friction problems, and more specifically, for difficult kinked and intersection crack geometries. The method is a combination of a successful frictional contact algorithm [25] based upon the SGBEM [28, 29], and the MQP crack tip element mentioned above. The goal is to demonstrate that this approach yields highly accurate SIFs, even with a simple local SIF method such as Displacement Correlation Technique. Moreover, accurate results are obtained without highly refined meshes, and thus fewer iterations are required to solve the nonlinear friction problem.

For completeness, the next section provides a brief review of Symmetric-Galerkin fracture analysis and the MQP element, while the SGBEM frictional contact algorithm is reviewed in Sect. 3. Section 4 presents the SIF results obtained using these methods for several crack configurations. These solutions are compared with either exact results or with numerical solutions obtained using a numerical method due to Gerasoulis [30] or the DDM [3]. Some concluding remarks are in Sect. 5.

2
SGBEM fracture analysis

This section provides a very brief review of boundary integral equations for elasticity, their approximation via the symmetric-Galerkin procedure, and the application to fracture. The reader is asked to consult the cited references for further details.

The boundary integral equation (BIE) without body forces for linear elasticity is given by Rizzo [31]. For a source point P interior to the domain, this equation takes the form

$$u_k(P) - \int_{\Gamma_b} \left[U_{kj}(P,Q)\tau_j(Q) - T_{kj}(P,Q)\, u_j(Q)\right] \mathrm{d}Q = 0 \ , \tag{1}$$

where Q is a field point, τ_j and u_j are traction and displacement vectors, U_{kj} and T_{kj} are the Kelvin kernel tensors or fundamental solutions, Γ_b denotes the boundary of the domain, and dQ is an infinitesimal boundary length (for 2-D) or boundary surface (for 3-D cases).

It can be shown that the limit of the integral in Eq. (1) as P approaches the boundary exists. From now on, for $P \in \Gamma_b$, the BIE is understood in this limiting sense.

As P is off the boundary, the kernel functions are not singular and it is permissible to differentiate Eq. (1) with respect to P, yielding the hypersingular BIE (HBIE) for displacement gradient. Substitution of this gradient into Hooke's law gives the following HBIE for boundary stresses:

$$\sigma_{k\ell}(P) - \int_{\Gamma_b} \left[D_{kj\ell}(P,Q)\, \tau_j(Q) - S_{kj\ell}(P,Q)\, u_j(Q)\right] \mathrm{d}Q = 0 \ . \tag{2}$$

Expressions for the kernel tensors $U_{kj}, T_{kj}, D_{kj\ell}$ and $S_{kj\ell}$ can be found in [28].

The Galerkin boundary integral formulation is obtained by taking the shape functions ψ_m employed in approximating the boundary tractions and displacements as weighting functions for the integral equations (1) and (2). Thus,

$$\int_{\Gamma_b} \psi_m(P)\, u_k(P) \mathrm{d}P - \int_{\Gamma_b} \psi_m(P) \int_{\Gamma_b} \left[U_{kj}(P,Q)\, \tau_j(Q) - T_{kj}(P,Q)\, u_j(Q)\right] \mathrm{d}Q\, \mathrm{d}P = 0 \ , \tag{3}$$

$$\int_{\Gamma_b} \psi_m(P)\, \sigma_{k\ell}(P) \mathrm{d}P - \int_{\Gamma_b} \psi_m(P) \int_{\Gamma_b} \left[D_{kj\ell}(P,Q)\, \tau_j(Q) - S_{kj\ell}(P,Q)\, u_j(Q)\right] \mathrm{d}Q\, \mathrm{d}P = 0 \ . \tag{4}$$

A symmetric coefficient matrix, and hence a symmetric-Galerkin approximation, is obtained by employing Eq. (3) on the boundary $\Gamma_{b(\mathbf{u})}$ where displacements u_{bv} are prescribed, and similarly using Eq. (4) is employed on the boundary $\Gamma_{b(\tau)}$ with prescribed tractions τ_{bv}. Note that $\Gamma_b = \Gamma_{b(\mathbf{u})} + \Gamma_{b(\tau)}$.

A solution procedure that employs a collocation approach enforces the BIE (1) and HBIE (2) at discrete source points whereas these equations are satisfied in an averaged sense with the Galerkin approximation. The additional boundary integration is the key to obtaining a symmetric coefficient matrix, as this ensures that the source point P and field point Q are treated in the same manner in evaluating the kernel tensors $U_{kj},\ T_{kj},\ D_{kj\ell}$ and $S_{kj\ell}$. After discretization, the resulting equation system can be written as

$$\begin{bmatrix} H_{11} & H_{12} \\ H_{21} & H_{22} \end{bmatrix} \begin{Bmatrix} u_{bv} \\ u_* \end{Bmatrix} = \begin{bmatrix} G_{11} & G_{12} \\ G_{21} & G_{22} \end{bmatrix} \begin{Bmatrix} \tau_* \\ \tau_{bv} \end{Bmatrix} \ . \tag{5}$$

Here, the first and second rows represent, respectively, the BIE written on $(\Gamma_{b(\mathbf{u})})$ and the HBIE on $(\Gamma_{b(\tau)})$. Further, u_* and τ_* denote unknown displacement and traction vectors. Rearranging Eq. (5) into the form $[A]\{x\} = \{b\}$, and multiplying the HBIE by -1, one obtains

$$\begin{bmatrix} -G_{11} & H_{12} \\ G_{21} & -H_{22} \end{bmatrix} \begin{Bmatrix} \tau_* \\ u_* \end{Bmatrix} = \begin{Bmatrix} -H_{11}u_{bv} + G_{12}\tau_{bv} \\ H_{21}u_{bv} - G_{22}\tau_{bv} \end{Bmatrix} \tag{6}$$

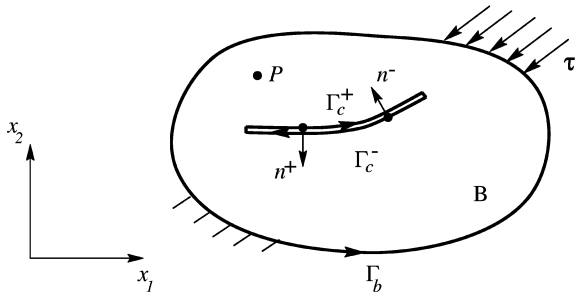

Fig. 1. A body B containing a fracture

The symmetry of the coefficient matrix, $G_{11} = G_{11}^T$, $H_{22} = H_{22}^T$ and $H_{12} = G_{21}^T$ now follows from the symmetry properties of the kernel tensors.

2.1 Cracks in finite domains

A finite domain or body, B, of general shape is shown in Fig. 1. The body is shown to include a crack surface denoted as Γ_c on which only tractions are prescribed. Initially, the crack is composed of two coincident surfaces according to $\Gamma_c = \Gamma_c^+ + \Gamma_c^-$ where Γ_c^+ and Γ_c^- denote the upper and lower crack surfaces, respectively. As a result, the outward normals to the crack surfaces, $\mathbf{n}_c^+$ and $\mathbf{n}_c^-$, are oriented oppositely so that $\mathbf{n}_c^- = -\mathbf{n}_c^+$. Thus, the BIE and HBIE written for an interior point P then take the following forms:

$$u_k(P) = \int_{\Gamma_b} \left[U_{kj}(P,Q)\,\tau_j(Q) - T_{kj}(P,Q)\,u_j(Q)\right] \mathrm{d}Q + \int_{\Gamma_c^+} \left[U_{kj}(P,Q)\,\Sigma\tau_j(Q) - T_{kj}(P,Q)\,\Delta u_j(Q)\right] \mathrm{d}Q \ , \tag{7}$$

$$\sigma_{k\ell}(P) = \int_{\Gamma_b} \left[D_{kj\ell}(P,Q)\,\tau_j(Q) - S_{kj\ell}(P,Q)\,u_j(Q)\right] \mathrm{d}Q + \int_{\Gamma_c^+} \left[D_{kj\ell}(P,Q)\,\Sigma\tau_j(Q) - S_{kj\ell}(P,Q)\,\Delta u_j(Q)\right] \mathrm{d}Q \ , \tag{8}$$

where, only the upper crack surface Γ_c^+ needs to be modeled as on the two crack surfaces, the displacements $\mathbf{u}_c^+$ and $\mathbf{u}_c^-$ are replaced by the single crack opening displacement (COD) $\Delta\mathbf{u}_c = \mathbf{u}_c^+ - \mathbf{u}_c^-$, and the tractions $\boldsymbol{\tau}_c^+$ and $\boldsymbol{\tau}_c^-$ by the sum of tractions $\Sigma\boldsymbol{\tau}_c = \boldsymbol{\tau}_c^+ + \boldsymbol{\tau}_c^-$. However, since the crack surfaces are usually symmetrically loaded, i.e $\boldsymbol{\tau}_c^- = -\boldsymbol{\tau}_c^+$, one gets

$$u_k(P) = \int_{\Gamma_b} \left[U_{kj}(P,Q)\,\tau_j(Q) - T_{kj}(P,Q)\,u_j(Q)\right] \mathrm{d}Q - \int_{\Gamma_c^+} T_{kj}(P,Q)\,\Delta u_j(Q)\mathrm{d}Q \ , \tag{9}$$

$$\sigma_{k\ell}(P) = \int_{\Gamma_b} \left[D_{kj\ell}(P,Q)\,\tau_j(Q) - S_{kj\ell}(P,Q)\,u_j(Q)\right] \mathrm{d}Q - \int_{\Gamma_c^+} S_{kj\ell}(P,Q)\,\Delta u_j(Q)\mathrm{d}Q \ . \tag{10}$$

It can be shown that a symmetric coefficient matrix can be achieved by using $\Delta\mathbf{u}$ as variables on Γ_c^+. Following the Galerkin approximation, the limit of (9) and (10) is taken as $P \to \Gamma_{b(\mathbf{u})}$ and $\Gamma_{b(\boldsymbol{\tau})}$, respectively. At this point, it is convenient to convert the stress equation (10) into a traction equation through the identity $\tau_k(P) = \sigma_{k\ell}(P)n_\ell(P)$, with $n_\ell(P)$ being the outward normal at P. After discretizing, the following system established from Eqs. (9) and (10) is obtained:

$$[G_{bb}]\{\tau_b\} = [H_{bb}]\{u_b\} + [H_{bc}]\{\Delta u_c\} \ , \tag{11}$$

where b and c denote the outer boundary and upper crack surface, respectively.

Since tractions are prescribed on the crack, only Eq. (10) is written for source points on Γ_c^+. Again, following the Galerkin approximation, the limit of (10) as $P \to \Gamma_c$, the conversion of (10) into a traction equation, and discretization, the result is

$$[G_{cb}]\{\tau_b\} - [G_{cc}]\{\tau_c^+\} = [H_{cb}]\{u_b\} + [H_{cc}]\{\Delta u_c\} \ . \tag{12}$$

Note that $\boldsymbol{\tau}_c^+$ now appears on the left hand side of Eq. (12) due to the limit process as $P \to \Gamma_c$. Combining Eqs. (11) and (12), the equation system of the problem can be written as follows:

$$\begin{bmatrix} H_{bb} & H_{bc} \\ H_{cb} & H_{cc} \end{bmatrix} \begin{Bmatrix} u_b \\ \Delta u_c \end{Bmatrix} = \begin{bmatrix} G_{bb} & 0 \\ G_{cb} & G_{cc} \end{bmatrix} \begin{Bmatrix} \tau_b \\ -\tau_c^+ \end{Bmatrix} \ , \tag{13}$$

where it can be proved that the coefficient matrix on the left hand side of (13) is also symmetric.

2.2 Cracks in unbounded domains

When an unbounded domain is considered and is subjected to uniform remote stress $\bar{\sigma}_{ij}$, Eq. (12) reduces to the following system:

$$-[G_{cc}]\{\tau_c^+\} = [H_{cc}]\{\Delta u_c\} \ , \tag{14}$$

where $\{\tau_c^+\}$ on the upper crack surface Γ_c^+ is now the superposition of the prescribed tractions directly applied on Γ_c^+ and the tractions $\bar{\sigma}_{ij}n_j^+$ due to the remote stresses $\bar{\sigma}_{ij}$. Note that n_j^+ are the components of the outward normal $\mathbf{n}_c^+$ to Γ_c^+.

2.3 Modified quarter-point element

For a crack geometry, the crack opening displacement (COD) Δu_k, $k = 1, 2$ in the neighborhood of the tip is [32, 33]

$$\Delta u_k(r,\theta) = b_k(\theta)r^{\frac{1}{2}} + c_k(\theta)r + d_k(\theta)r^{\frac{3}{2}} + \cdots \ , \tag{15}$$

where r, θ are the distance to, and the direction emanating from, the tip, respectively.

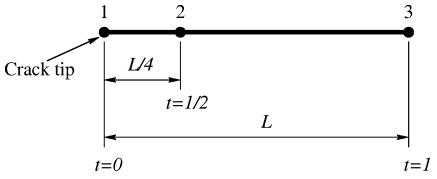

Fig. 2. Crack tip element

It has been proven that, irrespective of the problem geometry or boundary conditions, the series expansion in Eq. (15) must have $c_k = 0$ for $\Delta\mathbf{u}$ *on the crack surface* [10] (for related work see Ref. [34]), i.e.

$$\Delta u_k(r,\theta) = b_k(\theta) r^{\frac{1}{2}} + d_k(\theta) r^{\frac{3}{2}} + \cdots \quad . \tag{16}$$

It is known that the above equations have initially been established for crack opening. However, as these relationships are valid if there is an applied traction on the crack surface, they also apply for crack closure cases.

The 2-D QP element is based upon the three-equidistant-noded quadratic element. For $t \in [0, 1]$, the shape functions for this element are given by

$$\begin{aligned} \psi_1(t) &= (1-t)(1-2t) \quad , \\ \psi_2(t) &= 4t(1-t) \quad , \\ \psi_3(t) &= t(2t-1) \quad . \end{aligned} \tag{17}$$

As $\Delta\mathbf{u} = 0$ at the crack tip, which is assumed to be at $t = 0$ (Fig. 2), the geometry and COD representations of the crack tip element are

$$\Gamma(t) = \sum_{j=1}^{3} \Big(x_j \psi_j(t), y_j \psi_j(t) \Big) \quad , \tag{18}$$

$$\Delta u_k(t) = \sum_{j=2}^{3} \Big(\Delta u_1^{(j)} \psi_j(t), \Delta u_2^{(j)} \psi_j(t) \Big) \quad , \tag{19}$$

where (x_j, y_j) are the coordinates of the three nodes defining the crack tip element, and $\Delta u_k^{(j)}$ the nodal values of the COD.

By moving the mid-node coordinates (x_2, y_2) three-fourths of the way towards the tip (see Fig. 2), the parameter t becomes $\sqrt{r/L}$, with L being the distance from (x_1, y_1) to (x_3, y_3) [6, 7]. As a consequence, the leading order term in $\Delta u_k^{(j)}$ at $t = 0$, which is t, is the correct square root of distance. Note however, that the next term, which is t^2, is r/L. According to Eq. (16), this term should vanish, and the modification presented in Ref. [11] accomplishes the cancellation of this t^2 term. The resulting shape functions for the MQP element are

$$\begin{aligned} \hat{\psi}_2(t) &= -\tfrac{8}{3}(t^3 - t) \quad , \\ \hat{\psi}_3(t) &= \tfrac{1}{3}(4t^3 - t) \quad , \end{aligned} \tag{20}$$

which should be used in Eq. (19) instead of $\psi_j(t)$. It can be observed that the modified shape functions (20) still satisfy the Kronecker delta property $\hat{\psi}_i(t_j) = \delta_{ij}$. This new approximation is only applied to the COD, as we keep the representation of the crack tip geometry as in Eq. (18). This ensures that the property $t \approx \sqrt{r}$ remains.

2.4
Stress intensity factors

SIFs provided by both the modified and standard QP elements will be calculated by means of the DCT. The point here is to assess the quality of the MQP in the context of frictional contact fracture by means a very simple method such as the DCT. The general expressions of SIFs by means of the DCT technique are given by

$$\begin{aligned} K_I &= \frac{G}{\kappa+1} \lim_{r\to 0} \sqrt{\frac{2\pi}{r}} \Delta u_2 \quad , \\ K_{II} &= \frac{G}{\kappa+1} \lim_{r\to 0} \sqrt{\frac{2\pi}{r}} \Delta u_1 \quad , \end{aligned} \tag{21}$$

where $\Delta\mathbf{u}$ is the COD in the coordinate system associated with the crack tip under consideration, G is shear modulus, v is Poisson's ratio, and

$$\kappa = 3 - 4v \ \text{(plane strain)}, \quad \kappa = \frac{3-v}{1+v} \ \text{(plane stress)} \quad . \tag{22}$$

For the standard QP element, it is known that by substituting Eqs. (17) and (19) in Eq. (21), one gets

$$\begin{aligned} K_I &= \frac{G}{\kappa+1} \sqrt{\frac{2\pi}{L}} \Big(4\Delta u_2^{(2)} - \Delta u_2^{(3)} \Big) \quad , \\ K_{II} &= \frac{G}{\kappa+1} \sqrt{\frac{2\pi}{L}} \Big(4\Delta u_1^{(2)} - \Delta u_1^{(3)} \Big) \quad . \end{aligned} \tag{23}$$

The SIFs in case of the MQP element are obtained similarly [11], resulting in

$$\begin{aligned} K_I &= \frac{G}{3(\kappa+1)} \sqrt{\frac{2\pi}{L}} \Big(8\Delta u_2^{(2)} - \Delta u_2^{(3)} \Big) \quad , \\ K_{II} &= \frac{G}{3(\kappa+1)} \sqrt{\frac{2\pi}{L}} \Big(8\Delta u_1^{(2)} - \Delta u_1^{(3)} \Big) \quad . \end{aligned} \tag{24}$$

Thus, SIFs are given directly in terms of the nodal values of the COD at the crack tip element.

3
SGBEM crack friction algorithm

In this section we review the SGBEM algorithm for modeling cracks with frictional contact presented in [25]; further details can be found in this paper. Crack friction is a nonlinear boundary value problem that requires an iterative scheme. The SGBEM algorithm enables the determination of two important quantities, namely the normal tractions and crack sliding displacements (slip) on the sliding crack surfaces. Thus, a mode-II SIF can be found by using the slip result in Eq. (24). In the subsequent section, it is shown that the symmetric-Galerkin procedure can resolve problems of friction sliding in cases where the friction constraint condition may be different on each branch of a common junction point.

3.1
Problem formulation

Without loss of generality, consider an unbounded domain containing internal cracks subjected to prescribed

global tractions τ_c. As mentioned in Sect. 2.2, τ_c combines the prescribed tractions directly applied on crack faces and the tractions due to remote loading. Let Δu_n and Δu_t be, respectively, the crack opening/closing and sliding displacements in the local coordinate system (t, n). After the final solution of the iterative scheme is converged, additional local tractions $\mathbf{t} = (t_t, t_n)$ on the sliding crack surfaces are determined such that no material interpenetration occurs. Note that t_n and t_t are, respectively, the normal and tangential components of $\mathbf{t}$. The boundary conditions for the final solution are

1. Either $\Delta u_n = 0$ and $\Delta u_t = 0$ (the crack is not sliding), in which case $\mathbf{t} = 0$, or
2. $\Delta u_n > 0$ (the crack is open), also in which case $\mathbf{t} = 0$, or
3. Δu_n is forced to be 0 (no material interpenetration, the crack is sliding) by applying additional tractions $\mathbf{t}$ on those crack surfaces; the normal and tangential components of $\mathbf{t}$ are related by $|t_t| = -\tan(\phi) t_n$ with ϕ being the friction angle. The sign of t_t is such that the sliding movement of the crack surfaces is opposed.

Note that t_n is nonlinearly dependent on the Δu_n values on all other cracks and on the field stress.

3.2
Iterative procedure

For crack friction problems, the numerical solution with the initial traction boundary conditions on the crack surfaces provides negative Δu_n (material interpenetration) in the region of contact. This negative Δu_n solution is obviously unphysical, and thus an iterative procedure is employed to determine t_n and t_t such that $\Delta u_n \geq 0$.

1. From the SGBEM solution for the global COD $\Delta \mathbf{u}_c$, compute the local displacement components Δu_n and Δu_t.
2. If $\Delta u_n < 0$ at a given node on the crack, set
   (a) normal traction at the ith step as $t_n^{(i)} = t_n^{(i-1)} - k\Delta u_n$, where $t_n^{(i-1)}$ is the normal traction at the previous step, and $k = (\alpha G)/b$ with α, G and b being the relaxation factor, shear modulus and crack length, respectively,
   (b) $t_t = \text{sign}(\Delta u_t) \tan(\phi) t_n$.
3. At the crack tips of a sliding crack, normal tractions $t_n^{(i)}$ are determined by interpolating those at the other nodes of the crack tip elements.
4. Convert the local traction components t_n and t_t to the global traction vector τ_{ca}^+ on the upper crack surface.
5. Superpose the above additional tractions τ_{ca}^+ to the initially prescribed tractions τ_c^+ on the crack surface. Re-solve the SGBEM system.
6. Repeat from the first step until convergence.

The error indicator of convergence is calculated after each iterative step as the maximum difference between the current and previous computed local normal traction component

$$\epsilon = \max |t_n^{(i)} - t_n^{(i-1)}| \tag{25}$$

The iteration process is converged when the error indicator ϵ is below a specified tolerance ϵ_0.

Note that in applying the friction interface model, we have specified an inequality constraint that requires the friction resistance on the sliding interface to be greater than or equal to the shear stress acting across the interface. Consequently, the frictional contact problem does in general depend on the loading history and the solutions that satisfy this form of boundary condition are not necessarily unique. For example, if one of the existing solutions was considered and a small reverse slip was applied to a section of the sliding interface, then the inequality could still be satisfied although the "solution" would be different but still valid in terms of the stated boundary constraint. Here the path-dependency inherent in frictional contact problems is handled by a suitable routine that numerically implements Step 2(a) where an incremental load $k\Delta u_n$ is employed to adjust the normal traction t_n obtained from the previous step until no material interpenetration occurs. In addition, we do not treat explicit time dependent rate/state friction constitutive rules or general time dependent evolution of the solution. In order to provide a "sensible engineering" result, satisfying the boundary conditions, it is necessary therefore to consider all loading steps to be suitably "small" through the use of relaxation factor α and to be arranged in a defined sequence.

4
SIF calculations

As noted in the introduction, the purpose of this paper is to demonstrate that the above techniques produce accurate SIF results. Three problems are considered in this section, the last two involving kinked and junction cracks. Unless otherwise noted, the plane strain state is considered, the material constants employed are Young's modulus $E = 70000$ MPa and Poisson's ratio $\nu = 0.2$, and a convergence criterion $\epsilon_0 = 10^{-6}$ MPa is chosen.

4.1
Single crack under compression

A relatively simple geometry, a single crack of length $2b$ in an unbounded domain and subject to a compressive remote stress σ (see Fig. 3), is considered first, as an analytical solution is available for comparison. Results are presented for various inclination angles of the crack relative to the applied stress, denoted by α, and friction angles $\phi = 0°, 15°, 30°, 45°$.

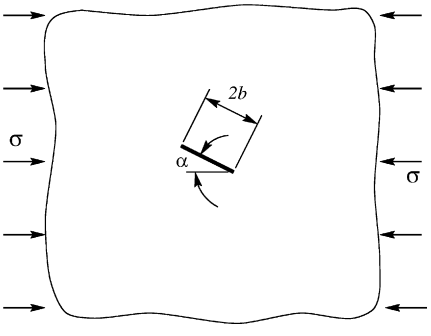

Fig. 3. A crack under compression in an unbounded domain

It is obvious that the mode-I SIF $K_I = 0$ as the crack surfaces remain closed under compression. The analytical solution for the mode-II SIF is given by [35]

$$K_{II} = \sigma\sqrt{\pi b}\sin\alpha(\cos\alpha - \tan\phi\sin\alpha) \ . \qquad (26)$$

For the first set of calculations, the crack is discretized into ten uniform quadratic elements. The numerical solution obtained with the MQP for $K_{II}/\sigma\sqrt{\pi b}$ (normalized K_{II}) is plotted in Fig. 4 together with the analytical solution. The solutions are almost identical. The performance of the MQP versus standard QP elements is compared in terms of the ratio $K_{II}/K_{II}^{\text{exact}}$ listed in Table 1 for different inclination and friction angles α and ϕ. While the accuracy is consistent regardless the values of α and ϕ, the solutions obtained with the MQP element are roughly three orders of magnitude more accurate than those obtained with the standard QP element. This remains valid for $\alpha = \phi = 45°$. However, a comparison in terms of $K_{II}/K_{II}^{\text{exact}}$ can not be shown as $K_{II}^{\text{exact}} = 0$ in this case.

The primary advantage of the MQP over standard QP element in solving crack friction problems is illustrated by the comparison shown in Table 2. This table reveals that, for equivalent accuracy, the mesh for the MQP calculation can be significantly coarser than that required by the standard QP element. This advantage has also been observed in Ref. [11] in the context of non contact crack modeling. However, this is much more significant in case of contact fracture, as the computing time required by the nonlinear iteration is very much mesh dependent. For the single crack under consideration, even a mesh of 100 elements with standard QP crack tip elements produces less accurate K_{II} result than that obtained from a mesh of only five crack elements with MQP crack tip elements. In addition, while the former case requires 2478 iterative steps, the latter only needs 178 steps. It is also interesting to note that with the same number of crack elements employed, the use of MQP element not only provides much more accurate solution, but also requires fewer iterative steps. This lower number of iterations might be explained by the more accurate solutions for crack opening and crack sliding displacements near the crack tips provided by the MQP element. Finally, note that the MQP solution accuracy actually decreases slightly for more than ten elements; this decrease may be explained by the fact that the crack tip element should be 'long enough' for the t^3 terms in the MQP shape functions (see Eq. (20)) to exhibit their presence [11]. However, the asymptotic value for K_{II} is still more accurate than the respective standard QP solution.

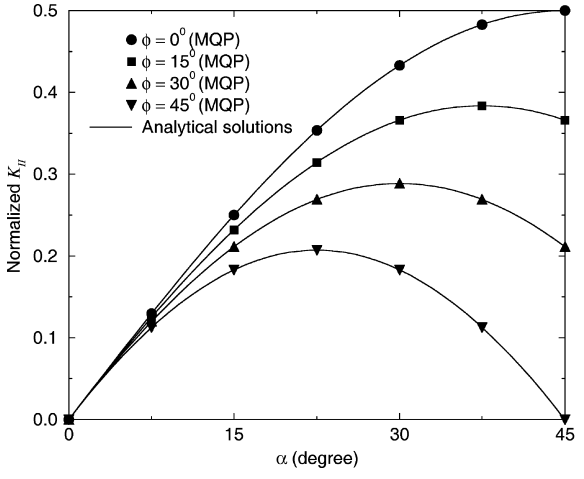

Fig. 4. Numerical results vs. analytical solutions for normalized K_{II}

Table 1. $K_{II}/K_{II}^{\text{exact}}$ as functions of inclination angle α and friction angle ϕ (10 crack elements)

Angle α	Crack tip element	Friction angle ϕ			
		0°	15°	30°	45°
15°	QP	1.02334	1.02334	1.02335	1.02335
	MQP	0.99994	0.99994	0.99994	0.99994
30°	QP	1.02334	1.02334	1.02334	1.02335
	MQP	0.99994	0.99994	0.99994	0.99994
45°	QP	1.02334	1.02334	1.02335	N/A
	MQP	0.99994	0.99994	0.99994	N/A

Table 2. $K_{II}/K_{II}^{\text{exact}}$ and number of iterative steps as functions of number of crack elements ($\alpha = 20°$ and $\phi = 30°$)

Number of crack elements	Crack tip element	$K_{II}/K_{II}^{\text{exact}}$	Number of iterative steps
5	QP	1.05015	186
	MQP	1.00144	178
10	QP	1.02335	329
	MQP	0.99994	319
20	QP	1.01097	607
	MQP	0.99961	585
30	QP	1.00698	866
	MQP	0.99956	836
40	QP	1.00500	1113
	MQP	0.99954	1079
50	QP	1.00383	1351
	MQP	0.99953	1313
75	QP	1.00227	1929
	MQP	0.99953	1871
100	QP	1.00149	2478
	MQP	0.99953	2403

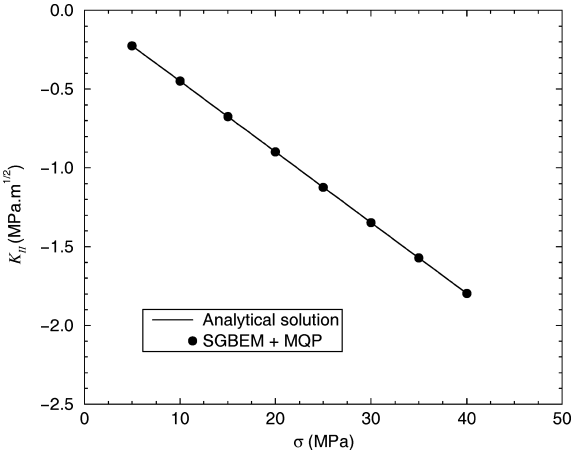

Fig. 5. Numerical results vs. analytical solutions for K_{II}

Table 3. $K_{II}/K_{II}^{\text{exact}}$ as a function of σ

Remote compressive stress σ (MPa)							
5	10	15	20	25	30	35	40
0.99994	0.99994	0.99994	0.99994	0.99994	0.99994	0.99994	0.99994

The performance of using the SGBEM and MQP element in modeling crack friction problems can also be demonstrated by comparing these SIF results with those obtained from FROCK [24]. Consider a single closed crack in an infinite medium (see Fig. 3) with $2b = 0.0127$ m, $\alpha = 45^\circ$ and $\tan\phi = 0.364$. For numerical analysis, the crack is discretized into ten uniform quadratic elements. Figure 5 shows the mode-II SIF results obtained from the exact solution K_{II}^{exact} and from SGBEM using the MQP element for different magnitudes of σ, while results for the ratio $K_{II}/K_{II}^{\text{exact}}$ are listed in Table 5. Again, these illustrations reveal that both solutions are almost identical. While the MQP solutions for K_{II} remain consistently accurate regardless any value of applied stress σ (see Table 3), those obtained from FROCK and shown in Ref. [24] appear to be less accurate when the remote compressive stress σ exceeds 20 MPa. Note that with frictional contact boundary conditions, the solution is not a linear function of the stress.

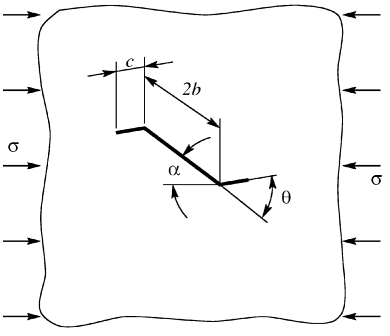

Fig. 6. Two-wing crack in an unbounded domain

4.2
Two-wing crack under compression

In this section, a two-wing crack in an unbounded domain and under uniaxial far-field compression as shown in Fig. 6 is investigated. This is the problem of kinked crack extension from an initially closed crack [36]. Due to the symmetry of this problem, SIFs at both crack tips are identical. The MQP element is employed to calculate these SIFs for different values of ratio c/b and kink angle θ, fixing orientation angle $\alpha = \pi/5$ and friction coefficient $\tan\phi = 0.3$. For numerical analysis by the SGBEM, non-uniform quadratic elements are used to discretize the initially closed crack and its two wings. This mesh refinement technique needs to be employed to treat the singularity in the dislocation densities at the crack kinks (junction points) [16].

The normalized SIF results ($K_I/\sigma\sqrt{\pi b}$ and $K_{II}/\sigma\sqrt{\pi b}$) are plotted in Figs. 7 and 8. It can be observed that these results agree very well with those presented in Ref. [36] where a numerical method due to Gerasoulis [30] is used to solve a singular integral equation derived for this problem. It should be noted that, for a given value of c/b, θ, α and ϕ, the wings remain closed when the angle θ is smaller than a certain value, and thus $K_I = 0$ in these cases (see Fig. 7). While the SGBEM K_I solution properly interprets this closure situation, the numerical method employed in [36] provides $K_I < 0$ which represents material interpenetration.

To provide reference data, Tables 4 and 5 list the values of the normalized SIFs used to build the graphs shown in Figs. 7 and 8, respectively.

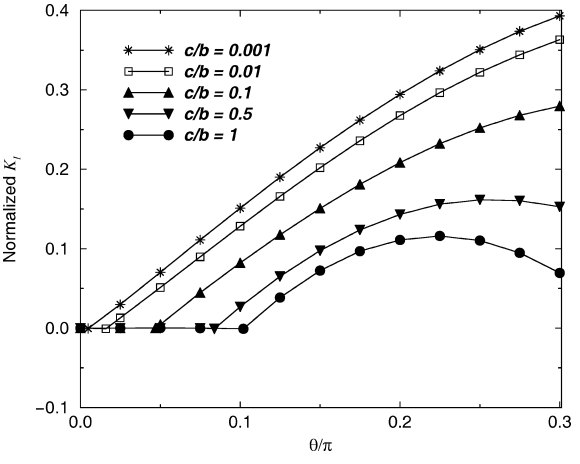

Fig. 7. Normalized K_I solution ($\alpha = \pi/5$, $\tan\phi = 0.3$)

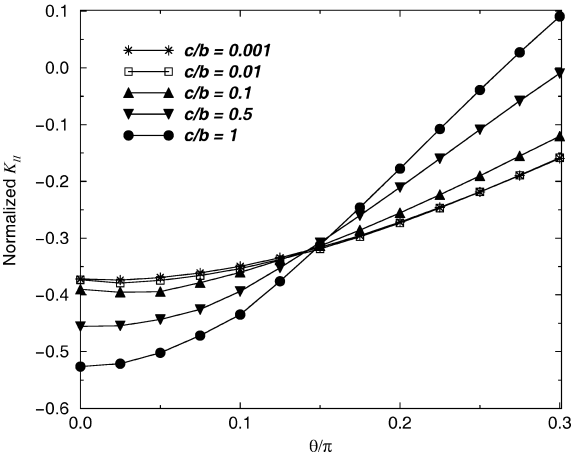

Fig. 8. Normalized K_{II} solution ($\alpha = \pi/5$, $\tan\phi = 0.3$)

4.3
T-crack problem

Finally, consider a T-crack in an unbounded domain and subject to a remote compressive stress $\sigma = 100$ MPa acting vertically (see Fig. 9). The lengths of the vertical (opening) and horizontal (sliding) crack segments of this kinked crack are $c = 100$ m and $2b = 50$ m, respectively. The vertical segment is horizontally pressurized to

Table 4. Numerical results for normalized $K_I(\alpha = \pi/5, \tan \phi = 0.3)$

θ/π	$5c/b$				
	0.001	0.01	0.1	0.5	1
0	−0.00009	−0.00009	−0.00009	−0.00010	−0.00009
0.025	0.02992	0.01298	−0.00009	−0.00009	−0.00009
0.05	0.07027	0.05102	0.00464	0.00001	0.00007
0.075	0.11101	0.08972	0.04444	−0.00008	−0.00009
0.1	0.15112	0.12830	0.08216	0.02684	−0.00097
0.125	0.18998	0.16600	0.11768	0.06528	0.03838
0.15	0.22710	0.20199	0.15089	0.09765	0.07241
0.175	0.26204	0.23608	0.18106	0.12356	0.09677
0.2	0.29446	0.26763	0.20843	0.14321	0.11110
0.225	0.32406	0.29638	0.23221	0.15596	0.11590
0.25	0.35054	0.32200	0.25211	0.16165	0.11035
0.275	0.37372	0.34431	0.26799	0.16063	0.09468
0.3	0.39344	0.36314	0.27964	0.15278	0.06967

Table 5. Numerical results for normalized $K_{II}(\alpha = pi/5, \tan \phi = 0.3)$

θ/π	c/b				
	0.001	0.01	0.1	0.5	1
0	−0.37202	−0.37369	−0.38999	−0.45554	−0.52620
0.025	−0.37404	−0.37926	−0.39505	−0.45443	−0.52103
0.05	−0.36960	−0.37432	−0.39404	−0.44354	−0.50206
0.075	−0.36139	−0.36573	−0.37875	−0.42558	−0.47183
0.1	−0.34963	−0.35350	−0.36019	−0.39353	−0.43455
0.125	−0.33455	−0.33780	−0.33844	−0.35234	−0.37576
0.15	−0.31637	−0.31906	−0.31352	−0.30764	−0.31242
0.175	−0.29537	−0.29733	−0.28610	−0.26030	−0.24588
0.2	−0.27185	−0.27312	−0.25582	−0.21054	−0.17751
0.225	−0.24613	−0.24673	−0.22365	−0.15973	−0.10775
0.25	−0.21860	−0.21861	−0.19010	−0.10895	−0.03899
0.275	−0.18964	−0.18912	−0.15554	−0.05842	0.02723
0.3	−0.15964	−0.15865	−0.12066	−0.00952	0.09041

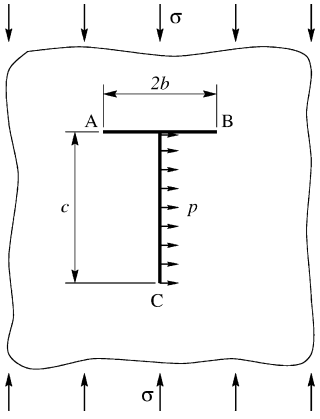

Fig. 9. A T-crack in an unbounded domain

$p = 100$ MPa internally and intersects the the middle of the horizontal segment at right angles.

The SGBEM and MQP element are used to compute SIFs at the tips A, B, and C for frictional angle $\phi = 30°$. The numerical results are compared with those obtained from the DDM using internal collocation [23]. For the DDM simulations, 50/200 and 100/400 uniform elements (mesh 1/mesh 2) are employed to discretize the horizontal and vertical cracks, respectively. For the SGBEM calculations, the corresponding numbers of elements are only 26 and 41. Again, as this is a kinked crack problem, mesh refinement technique needs to be used for the SGBEM analysis, with shorter elements being placed near the junction point. SIF results from both methods are listed in Table 6. Note that due to symmetry, at crack tips A and B, $K_{IIA} = -K_{IIB}$. Very good agreement from the numerical solutions can be observed. However, DDM needs to use a highly refined mesh to obtain the equivalent accuracy obtained by a coarser SGBEM mesh.

Table 6. SIFs at crack tips C and A

	$K_{IC}/p\sqrt{\pi c}$	$K_{IIA}/\sigma\sqrt{\pi b}$
DDM (mesh 1)	0.7212	1.16E-3
DDM (mesh 2)	0.7169	4.25E-3
SGBEM	0.7166	2.65E-3

5 Conclusion

The SGBEM combined with a simple frictional contact algorithm and the MQP crack tip element provides an efficient approach for accuarately evaluating SIFs for fractures with frictional sliding. Two important advantages of the SGBEM are exploited, namely the ability to use standard continuous elements to solve crack problems, and the ability to accurately handle corners and junction points. As a result, the elegant quarter-point element can be employed to accurately capture the crack tip singularity, and a simple iterative scheme proposed in Ref. [25] can be adopted to solve crack friction problems. Of particular interest herein was the investigation of difficult kinked or junction crack geometries, and it was found that they do not appear to pose any problems. SGBEM results are almost identical to the analytical solutions for the problem of single crack under compression; and agree very well with a numerical method due to Gerasoulis [30] for the problem of two-wing crack under compression. A key advantage of the MQP is that accurate results can be obtained without refined meshes. This meshing advantage is amplified for nonlinear crack friction analysis, as the solution requires an iterative procedure.

The DDM, employed in the T-crack example to provide comparison with the SGBEM results, requires refined mesh to yield comparable accuracy obtained by a coarser SGBEM mesh. Due to the use of internal collocation, it is expected that the 'non-conforming' DDM will be, compared to SGBEM, even more computationally expensive in treating 3-D problems. Extension of this work to three dimensions is currently in progress.

References

1. **Cook RD, Malkus DS, Plesha ME** (1989) Concepts and Applications of Finite Element Analysis. John Wiley & Sons, New York

2. **Cruse TA** (1988) Boundary Element Analysis in Computational Fracture Mechanics. Kluwer Academic Publishers, Boston
3. **Crouch SL, Starfield AM** (1990) Boundary Element Methods in Solid Mechanics. Unwin Hyman, London
4. **Aliabadi MH** (1997) Boundary element formulations in fracture mechanics. Appl. Mech. Rev. 50: 83–96
5. **Chen JT, Hong H-K** (1999) Review of dual boundary element methods with emphasis on hypersingular integrals and divergent series. Appl. Mech. Rev. 52: 17–33
6. **Henshell RD, Shaw KG** (1975) Crack tip finite elements are unnecessary. Int. J. Numer. Meth. Eng. 9: 495–507
7. **Barsoum RS** (1976) On the use of isoparametric finite elements in linear fracture mechanics. Int. J. Numer. Meth. Eng. 10: 25–37
8. **Blandford GE, Ingraffea AR, Liggett JA** (1981) Two-dimensional stress intensity factor computations using the boundary element method. Int. J. Numer. Meth. Eng. 17: 387–404
9. **Banks-Sills L** (1991) Application of the finite element method to linear elastic fracture mechanics. Appl. Mech. Rev. 44: 447–461
10. **Gray LJ, Paulino GH** (1998) Crack tip interpolation, revisited. SIAM J. Appl. Math. 58: 428–455
11. **Gray LJ, Phan A-V, Paulino GH, Kaplan T** (2003) Improved quarter-point crack tip element. Eng. Fract. Mech. 70: 269–283
12. **Johnson KL, Shercliff HR** (1992) Shakedown of 2-dimensional asperities in sliding contact. Int. J. Mech. Sci. 34: 375–394
13. **Man KW, Aliabadi MH, Rooke DP** (1993) BEM frictional contact analysis: load incremental technique. Comput. Struct. 47: 893–905
14. **Huesmann A, Kuhn G** (1995) Automatic load incrementation technique for plane elastoplastic frictional contact problems using boundary element method. Comput. Struct. 56: 733–744
15. **Ingraffea AR, Heuze FE** (1980) Finite element models for rock fracture mechanics. Int. J. Numer. Anal. Meth. Geomech. 4: 25–43
16. **Zang WL, Gudmundson P** (1990) Contact problems of kinked cracks modelled by a boundary integral method. Int. J. Numer. Meth. Eng. 29: 847–860
17. **Zang WL, Gudmundson P** (1991) Frictional contact problems of kinked cracks modelled by a boundary integral method. Int. J. Numer. Meth. Eng. 31: 427–446
18. **Chen T-C, Chen W-H** (1998) Frictional contact analysis of multiple cracks by incremental displacement and resultant traction boundary integral equations. Eng. Anal. Bound. Elem. 21: 339–348
19. **Liu SB, Tan CL** (1992) Two-dimensional boundary element contact mechanics analysis of angled crack problems. Eng. Frac. Mech. 42: 273–288
20. **Lee SS** (1996) Analysis of crack closure problem using the dual boundary element method. Int. J. Frac. 77: 323–336
21. **Chan HCM, Li V, Einstein HH** (1990) A hybridized displacement discontinuity and indirect boundary element method to model fracture propagation. Int. J. Frac. 45: 263–282
22. **Shen B, Stephansson O** (1994) Modification of the G-criterion for crack propagation subjected to compression. Eng. Frac. Mech. 47: 177–189
23. **Napier JAL, Malan DF** (1997) A viscoplastic discontinuum model of time-dependent fracture and seismicity in brittle rock. Int. J. Rock Mech. Mining Sci. 34: 1075–1089
24. **Bobet A, Einstein HH** (1998) Numerical modeling of fracture coalescence in a model rock material. Int. J. Frac. 92: 221–252
25. **Phan A-V, Napier JAL, Gray LJ, Kaplan T** (2003) Symmetric-Galerkin BEM simulation of fracture with frictional contact. Int. J. Numer. Meth. Eng. 57: 835–851
26. **Gray LJ** (1991) Evaluation of hypersingular integrals in the boundary element method. Math. Comput. Modelling 15: 165–174
27. **Martin PA, Rizzo FJ** (1996) Hypersingular integrals: how smooth must the density be? Int. J. Numer. Meth. Eng. 39: 687–704
28. **Bonnet M** (1995) Boundary Integral Equation Methods for Solids and Fluids. John Wiley & Sons, England
29. **Bonnet M, Maier G, Polizzotto C** (1998) Symmetric Galerkin boundary element method. ASME Appl. Mech. Rev. 51: 669–704
30. **Gerasoulis A** (1982) The use of piecewise quadratic polynomials for the solution of singular integral equations of Cauchy type. Comput. Math. Appl. 8: 15–22
31. **Rizzo FJ** (1967) An integral equation approach to boundary value problems of classical elastostatics. Quart. Appl. Math. 25: 83–95
32. **Williams ML** (1952) Stress singularities resulting from various boundary conditions in angular corners of plates in extension. ASME J. Appl. Mech. 19: 526–528
33. **Williams ML** (1957) On the stress distribution at the base of a stationary crack. ASME J. Appl. Mech. 24: 109–114
34. **Martin PA** (1991) End-point behavior of solutions to hypersingular equations. Proc. R. Soc. Lond. A, 432: 301–320
35. **Melville PH** (1977) Fracture Mechanics of brittle materials in compression. Int. J. Frac. 13: 532–534
36. **Nemat-Nasser S, Horii H** (1982) Compression-induced nonplanar crack extension with application to spitting, exfoliation, and rockbust. J. Geophys. Res. 87: 6805–6821